Progress In Electromagnetics Research C, Vol. 131, 209–225, 2023

High-Gain Pixel Patch Antenna Array for Miniature Wireless Communications and IoT Applications

Yasser M. Madany[1, *], Hassan M. Elkamchouchi[1], and Sara I. Abd-Elmonieum[2]

Abstract—Since wireless technology has been developed so quickly, there is a surge in interest in multi-band reconfigurable antennas as devices and satellites continue to advance in the direction of downsizing. Due to physical limitations, current and future wireless technologies as well as the cutting-edge compact satellites need antenna systems that are dependable, effective, and have a large bandwidth. The fifth generation of mobile communication technology promises to deliver fast data rates, low latency, and exceptional spectrum efficiency. One of the most crucial factors that makes this technology possible is the way in which satellite technology is integrated with terrestrial communication systems. Therefore, it is crucially important to develop next-generation antennas that can meet the functional requirements for 5G and CubeSat applications. Additionally, the antenna components need to be small and low-profile for Advanced Driver-Assistance Systems (ADAS) and Vehicle-to-Everything (V2X) to function properly. Reconfigurable antennas can offer a wide range of configurations in terms of operating frequency, radiation pattern, and polarization. This paper aims to investigate pixel antenna arrays for wireless communication and Internet of Things (IoT) systems. Design, analysis, and comparison have been done on both the traditional and proposed pixel design configurations. The proposed pixel patch design area reduction is about 75%, and the full design area reduction is about 90%, compared to conventional patches. The pixel design parameters of these antennas are carefully examined to increase their gain, radiation pattern, and efficiency. For a variety of applications, increased gain and various radiation pattern configurations may be advantageous. As a result, increasing the coverage of 5G, 6G, and small satellites requires antennas with a small size, higher gain, and better radiation patterns.

1. INTRODUCTION

To meet the rising demand for data and connectivity, 4G wireless network is being replaced by the 5G network, which fixes issues brought on by previous network generations, including high energy consumption, lack of spectrum, inadequate coverage, and Quality of Service (QoS), increased capacity, global coverage, higher availability, and greater adaptability at multiple gigabits per second with a latency of one millisecond or less. For 5G to integrate existing communication technologies and utilize each to create a sizable heterogeneous network, it must deliver the performance necessary to satisfy regional and global market demands [1]. As a result, 5G will be able to deliver the necessary performance while meeting regional and global market demands. Mobile and satellite communication are examples of these technological developments. For 5G global connectivity to be possible, satellite communication networks are crucial because they make it possible to deploy networks quickly, effectively, and efficiently. Utilizing these benefits will increase the network's ability to broadcast worldwide, reduce reliance on terrestrial infrastructure, and provide high security. More than terrestrial-only solutions,

Received 15 February 2023, Accepted 18 March 2023, Scheduled 30 March 2023

* Corresponding author: Yasser M. Madany (ymadany@ieee.org).

[1] Communications and Electronics Department, Alexandria University, Alexandria, Egypt. [2] Electronics and Communications Department, College of Engineering and Technology, Arab Academy for Science, Technology & Maritime Transport, Alexandria, Egypt.

a 5G satellite-terrestrial network can enhance use cases. This can be accomplished by incorporating satellite communications into 5G. This covers private mobile and nomadic deployment, on-premises local networks, content acquisition and distribution, highly dispersed Internet of Things (IoT) networks, and on-premises local networks. Wireless devices must meet strict QoS requirements and transmit data at high rates over a variety of Wireless Communications Services (WCS) in IoT applications. These devices should be able to carry out several tasks at once and across WCS. Most often, reversible antennas are required. A wireless device demonstrates the capacity for dialogue in a range of contexts [2].

Traditional satellite architecture can be reduced, as demonstrated by nanosatellites. Any spacecraft with a diameter under one meter is considered a satellite. Previously enormous, intricate, time-consuming, and expensive satellite systems can now be developed as smaller, less expensive satellite structures in less time thanks to improvements in miniaturization techniques for electrical and electronic components. CubeSats make up most nanosatellites [3]. Nanosatellites are miniature satellites. CubeSats have a form factor of one Unit (1U). Depending on user requirements, this modular design can be scaled to 3U, 6U, 12U, or 24U. Commercially available Off-The-Shelf (COTS) components make the construction of CubeSats less complicated. Traditional satellites offer security, ubiquity, and coverage for 5G. Traditional satellite development for 5G communication is costly and time-consuming. Specialized knowledge and infrastructure are needed for design, development, and testing [4]. Satellites in Low Earth Orbit (LEO) are necessary for the IoT and massive Machine-Type Communication (mMTC) in next-generation communication systems like 5G and 6G. They must also communicate in constellations to offer mobility and global coverage [5].

The deployment of 6G technology, which is anticipated to begin in 2030, may be delayed by the lengthy and expensive construction of these massive conventional satellite constellations. Due to their small size and affordable development and launch costs, nanosatellites could be used to support satellite-terrestrial 5G networks in LEO. Their launch is reasonably priced because they can be launched from the International Space Station (ISS) or in "ridesharing" missions. To increase latency, robustness, security, and global coverage, nanosatellite constellations can be created and launched [6]. Compared to larger satellites, nanosatellites are simpler, less expensive, and easier to launch. The antenna was initially employed as a beam-emitting "pixel" on a surface. A pixel antenna's ability to function depends on its pixels. When being connected, pixels are metallic sub-wavelength sections that emit radiation and produce antenna impedance. The majority of currently used pixel antennas have square pixels. However, not all pixels are square. The pixel can be non-square if a plane tessellation can be created by copying the fundamental shape. By fusing volumetric pixels with switches, pixel antennas can create three-dimensional structures [7–10]. This study examines pixel antenna arrays for IoT and wireless communication systems. Both the traditional and the proposed pixel patch antenna configurations have been fabricated and measured. To illustrate the effectiveness of a new Driven-Shorting (DS) post strategy in antenna size reduction with lower-order mode, simulated and measured results of traditional and proposed antennas are compared. Such pixel antennas' design parameters are carefully examined to increase gain and enhance radiation pattern and efficiency [11]. Reconfigurable antennas with adjustable gain and radiation patterns are essential for extending 5G and microsatellite coverage [12, 13]. Different radiation pattern setups and increased gain can be beneficial.

2. TRADITIONAL PATCH ELEMENT DESIGN STRUCTURES

In this section, the traditional patch antenna design is shown and analyzed for some operating frequencies around 5 GHz using two different feed methods: microstrip-line and inset-feed. A dielectric substrate called Rogers Duroid 6010 with a relative permittivity of 10.2, a thickness of 0.635 mm, and a loss tangent of 0.0023 has been used to design the entire patch antenna. Based on the formulas in [14–16], Fig. 1 shows the sizes of traditional patch antennas in millimeters. They have a bottom layer that acts as a ground plane and has the same size as the dielectric.

After comparing the sizes of traditional patch antennas fed by two different methods, the traditional inset-fed patch antenna will be used as an example of the traditional designs. Using commercial software [17] that is based on the finite element method, simulation results for a traditional inset-fed patch antenna can be shown, such as scattering parameter, S_{11}, in dB, input impedance, Z_{in}, in ohms, and radiation characteristics, as shown in Fig. 2.

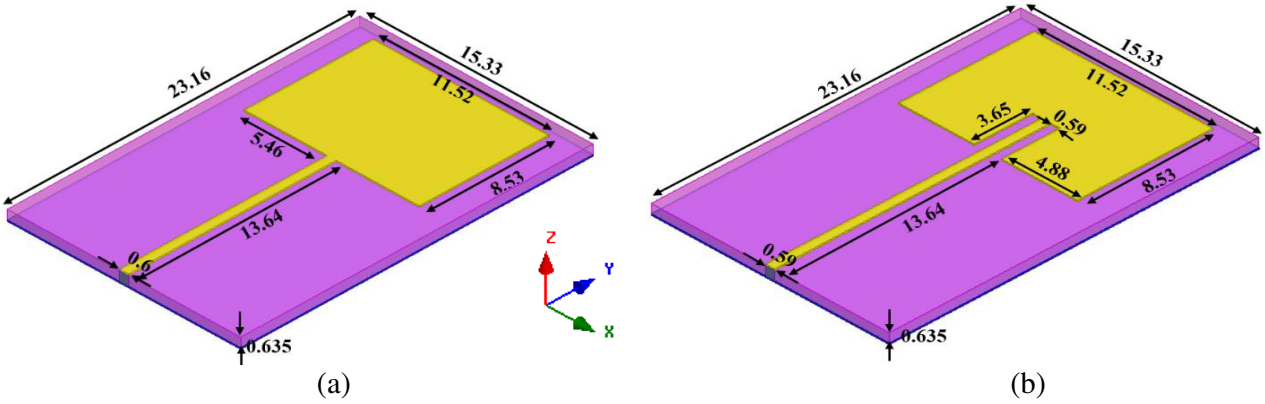

Figure 1. The traditional patch element dimensions in mm. (a) Microstrip-line. (b) Inset-fed.

The traditional inset-fed patch antenna element has a simulation return loss of −25 dB, a voltage standing wave ratio (VSWR) of roughly 1.12, and perfect impedance matching at the frequency of $f = 5.36$ GHz. The zero mode of excitation (TM_{01} or TM_{10}) is generally determined by the polarization plane in which the electric field varies due to the surface current distribution, as shown in Fig. 2, while the direction of the field variation determines which one will be excited. Due to field variation in the x-direction for microstrip-line feeding, the zero mode is TM_{01}, whereas for inset-feed, the zero mode is TM_{10} due to field variation in the y-direction. The configuration of the traditional patch antenna was designed and implemented, as shown in Fig. 3. At frequencies between 1 and 10 GHz, and ROHDE & SCHWARZ's ZVB-20 vector network analyzer was used to conduct all the measurements. In Fig. 3, photographs of the antenna laboratory's designed traditional antenna structure are demonstrated.

3. PIXEL PATCH ELEMENT DESIGN STRUCTURE

This antenna works at a frequency of about 5 GHz. The presentation and analysis of an electrically loaded small pixel patch design will be done around this frequency using a novel design strategy indicated by the microstrip antenna's DSpost. The dielectric substrate used in the suggested element structure is Rogers Duroid 6010, which has a thickness of 0.635 mm, a relative permittivity of 10.2, and a loss tangent of 0.0023. The size of the proposed pixel patch is in the range of $\lambda/4q$, where q is a rational number related to the root of the substrate's dielectric constant ($q \approx \sqrt{\varepsilon_r}$). A partially grounded, 1 mm-wide, 6 mm-long microstrip Transmission Line (TL) forms the bottom layer. q reduces the size of the pixel patch to highlight its importance and function. The patch measured about 5 mm, and q is roughly 3.2 [18]. Operating frequency differences can be eliminated during design by "matching." Fig. 4 depicts the proposed design geometry, and the parameters are tabulated in Table 1.

Table 1. The pixel patch element design parameters.

Parameter	Value	Unit
Operating frequency	5.32	GHz
Feeding technique	Probe feeding	
Pixel element patch width (W)	5	mm
Pixel element patch length (L)	5	
Pixel element substrate width/length (ℓ)	6	
TL start position from patch edge (m)	2	
Shorting post position (x_0, y_0)	$(0, 0.9)$	
Driven post position (x, y)	$(0, 0)$	

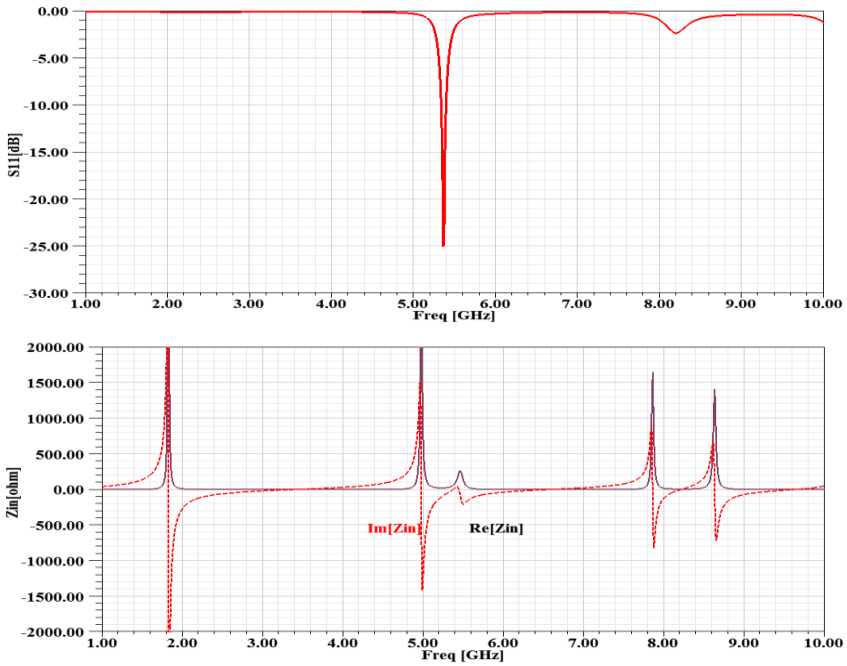

(a)

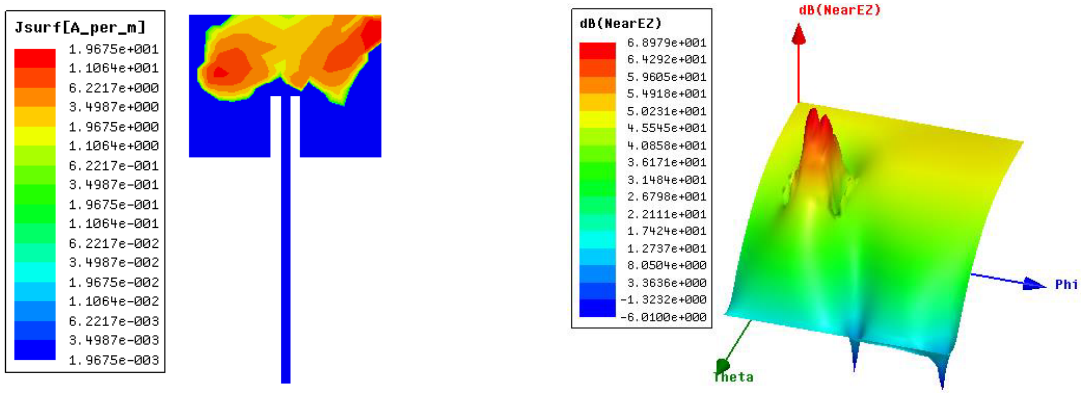

(b)

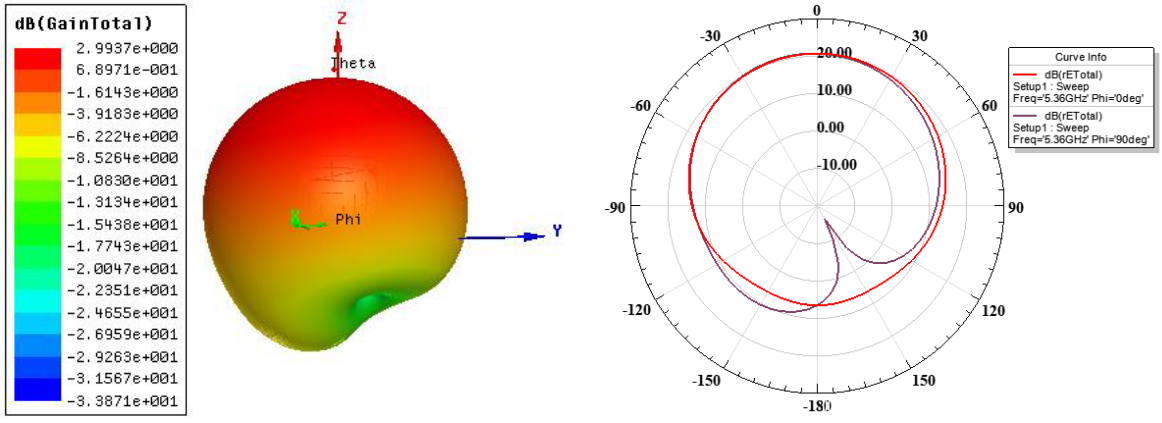

(c)

Figure 2. The traditional patch element scattering parameters and radiation characteristics. (a) S_{11} [dB], and Z_{in} [ohms], (b) near-field, E_z, and current distribution, $J_{surf.}$, and (c) 3D gain and total field.

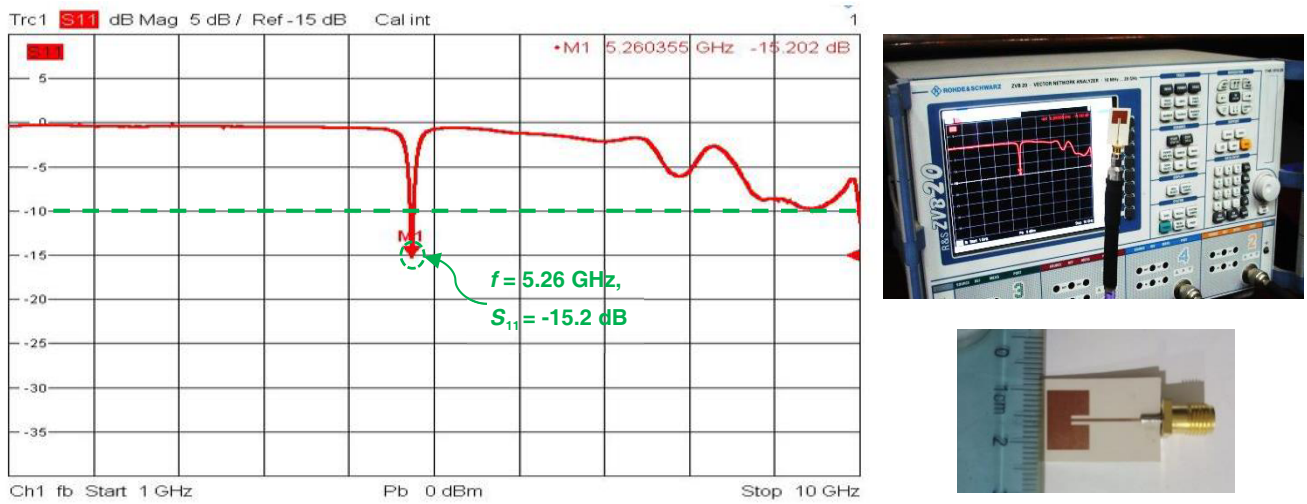

Figure 3. The fabricated sample of the traditional patch antenna element configuration and measurement results.

The analysis of the q parameter and its relationship to the operating frequency and patch length dimension for a relative permittivity is shown in Fig. 5. The static mode, denoted by zero mode, the dominant mode, denoted by resonant mode, the first higher mode, and the remaining higher order modes all have negligible losses due to higher resistance. The lossy substrate in the zero mode is accounted for by the static capacitance of the patch with a shunt resistance. The resonant mode can be expressed using a parallel RLC network. Additionally, the first higher mode can be represented by a similar RLC network, and all higher modes can be represented by a single inductor. As a result, using the zero mode of the unloaded microstrip antenna is necessary to comprehend and demonstrate the existence of a new resonance mode caused by a new DS-post. This new resonance mode can be represented by the inductance connected in series with the zero-mode static capacitances. Consider the general case of a shorting post connecting the top patch to the ground plane and a driven post fed by a coaxial line to concentrate on the working analysis of the driven-shorting post. The two posts have the same height, h, with a driven post fed position at (x, y) and a shorting post position at (x_0, y_0). S stands for the distance between the two posts, and d_{sp} and d_{dp}, respectively, stand for the diameters of the shorting post and driven post. The pixel patch antenna's posts are configured as shown in Fig. 5.

The analysis operates in two distinct modes: TL-mode and antenna-mode. In TL-mode, the charges move outward (in the opposite direction) with zero current on the top patch while experiencing maximum acceleration and instantaneous separation. The input impedance of this structure is determined for the antenna mode by comparing the voltage and current across the feed and the thin posts. The driven-shorting post's S, or the separation between the two posts, is very small and very close to zero. Therefore, for the TL-mode, the transmission line's effective length, ℓ, tends to equal the posts' height, h, and for the antenna mode with a DS-post, the scattering impedances are equal, as shown in Algorithm 1.

The outcomes of a simulation analysis using commercial software [17] are illustrated in Fig. 6 to determine the scattering parameters for the entire suggested configuration. This analysis was done to show if the proposed structure for the pixel patch elements could work. According to Fig. 6 and the inferences made from it, the new approach of using driven-shorting posts and the lower mode operation that were introduced in this paper achieved a different and more modern technique for reducing the patch antenna size while still enabling it to operate at higher operating frequencies. The proposed pixel patch element has a return loss of roughly -23 dB, a VSWR of 1.16, and perfect impedance matching at the frequency of $f = 5.32$ GHz. The radiation characteristics can be used as an illustration to better understand how the proposed pixel element functions. The patch surface current distribution, gain, and 3D total field are also demonstrated.

With the adoption of an SMT (antenna side) to SMA (vector network analyzer) RF connection after calibration to remove any potential interference with the proposed antenna test, the measurement setup

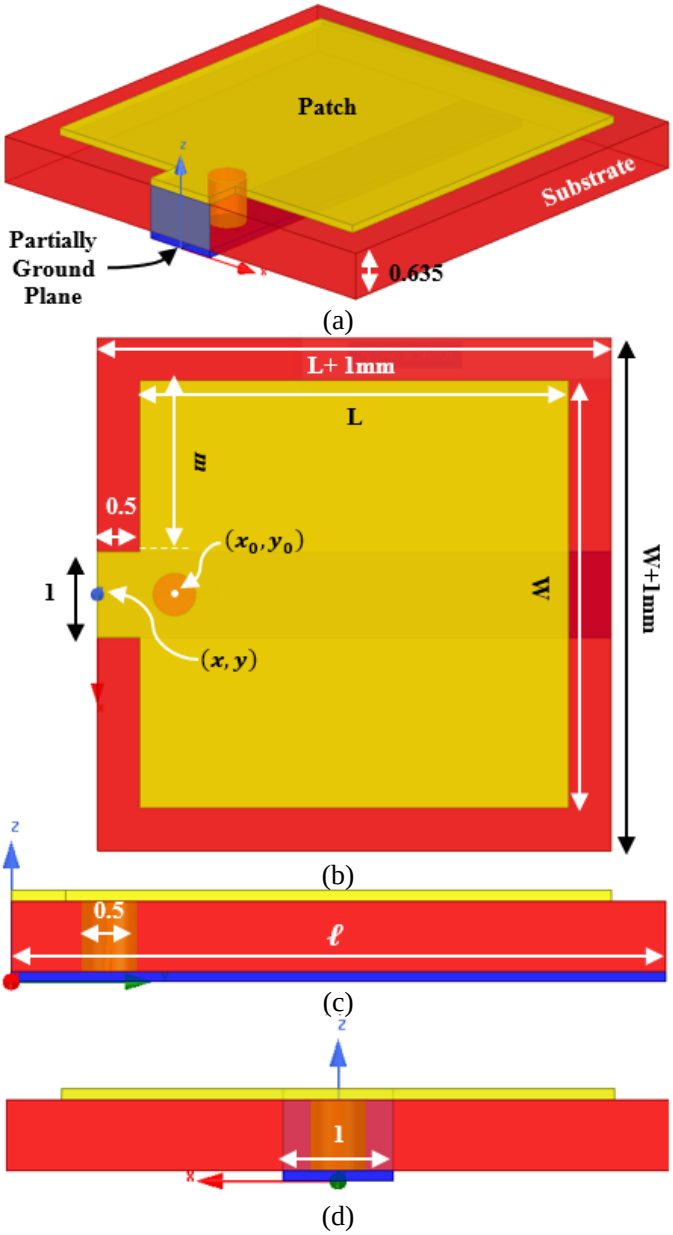

Figure 4. The main proposed pixel patch element parameters and dimensions in mm. (a) 3D view, (b) top view, (c) y-z view, (d) x-z view.

is the same as it would be for any other antenna. All measurements were made using the vector network analyzer ZVB-20, and they covered all frequencies between 1 and 10 GHz. Fig. 7 shows photographs and measurements of a sample of the proposed antenna design that was built and tested in an antenna laboratory. Lastly, Table 2 shows that the proposed antenna design has a smaller size and a lower order mode than traditional antenna designs.

Numerous references have demonstrated that the antenna's bandwidth and effectiveness will be impacted by the miniaturization of the antenna. Slot cutting [19–21], material loading [14, 22–26], ground plane modifications [27–37], metamaterials [38–40], shorting, folding [41–51], and hybrid techniques [52–58] have all been used to reduce the size of patch antennas. Also, it was found that each method changed the patch antenna's different properties when it was used. While miniaturization was successful, other qualities like bandwidth were sacrificed. Additionally, while some of the models

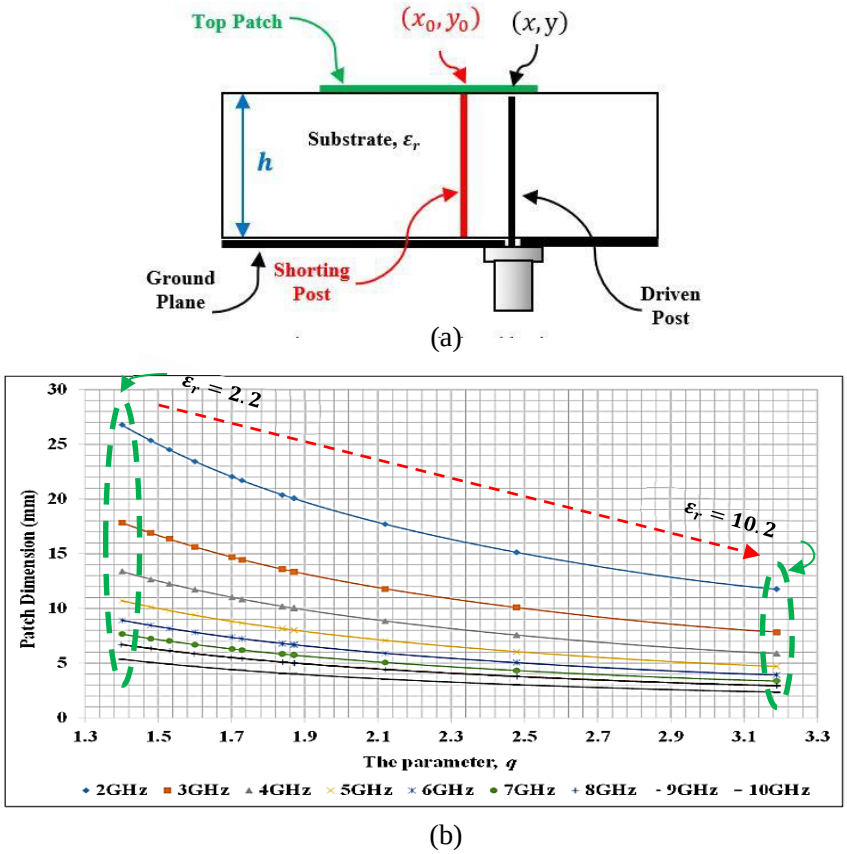

Figure 5. The pixel patch structure design. (a) Interior side view. (b) The parameter q analysis.

Table 2. Summary of the traditional and proposed pixel antenna design configurations.

Antenna Type	Feed Method	Mode(s) order	Patch Area (mm^2)	Antenna Area (mm^2)
Traditional	T. L.	Zero and Higher	98.3	355
	Inset-fed	Zero	91.8	355
Proposed	Coaxial	Lower	25	36

were simple to construct, others had very intricate shapes. A sample of some literature methods are compared with the proposed pixel patch antenna, and the summaries of these comparisons are listed in Table 3.

4. PIXEL ANTENNA ARRAY STRUCTURE

The individual pixel patch elements that make up pixel antenna arrays are frequently quite small. However, the geometric spacing between the elements and the relative amplitude and phase of the excitation currents on each element have a significant impact on the pattern of the array. Although the discrete sources radiate independently, the combination of these three elements results in the pattern of the array. The total radiation pattern is obtained by dividing the pattern of a single element by the pattern of the array (presuming point sources). A schematic of the proposed 5×5-pixel antenna array is shown in Fig. 8.

This design allows for independent control of amplitude and phase because each pixel patch is

Algorithm 1. The Driven-Shorting Post Impedance Analysis

Given: The operating frequency, $\boldsymbol{f}$, relative permittivity, $\boldsymbol{\varepsilon}$, relative permeability, $\boldsymbol{\mu_0}$, posts' height, $\boldsymbol{h}$, separation between the two posts, $\boldsymbol{S}$, the effective dimensions of the patch in x and y directions, $\boldsymbol{D_1}$, and $\boldsymbol{D_2}$, the diameters of the shorting post and driven post, $\boldsymbol{d_{sp}}$ and $\boldsymbol{d_{dp}}$, the intrinsic impedance, $\boldsymbol{\eta_0}$, and the electric field mode vectors, $\boldsymbol{\psi_{mn}}$ (precalculation):

1. Compute the eigen-value contributing to the right hand-side, $\boldsymbol{k}$, and $\boldsymbol{k_{mn}}$:
$$k = \omega\sqrt{\mu_0 \varepsilon}\ ,\ \varepsilon = \varepsilon_0 \varepsilon_r \tag{1}$$
$$k_{mn}^2 = k_m^2 + k_n^2\ ,\ k_m = \frac{m\pi}{D_1}\ ,\ k_n = \frac{n\pi}{D_2} \tag{2}$$
2. Determine the zero-mode capacitance and inductance:
   a. capacitance, $\boldsymbol{C}$:
$$C = \varepsilon \cdot \frac{1}{h \cdot |\psi_{00}(x_0, y_0)|^2} \tag{3}$$
   b. inductance, $\boldsymbol{L}$:
$$L = \mu_0 h \sum_{(m,n)\neq(0,0)} \frac{|\psi_{mn}(x_0, y_0)|^2}{k^2 - k_{mn}^2} \tag{4}$$
3. Compute the proposed design input impedance at the port, as $\boldsymbol{Z_{in} = 2\ Z_{TL}}$:
   a. phase constant, $\boldsymbol{\beta}$:
$$\beta = \omega\sqrt{LC} \tag{5}$$
   b. effective length of the transmission line, $\boldsymbol{\ell}$:
$$\ell = h + \frac{S}{\left(1 + \frac{r}{h}\right)}\ , r = \sqrt{D_1^2 + D_2^2} \tag{6}$$
   c. characteristic impedance, $\boldsymbol{Z_0}$:
$$Z_0 = \frac{\eta_0}{\pi} \cosh^{-1} \frac{S}{2\sqrt{d_{sp}.d_{dp}}} \tag{7}$$
4. For a short circuited two-wire transmission line formed by the vertical posts, $Z_L = 0$, (TL-mode):
$$Z_{TL}\big|_{Z_L=0} = j\ Z_0 \tan(\beta \ell) \tag{8}$$
5. Relating voltage and current across the thin driven and shorting posts, $V_1 = 0$, (antenna-mode):
$$V_2 = \left[\frac{Z_{11}Z_{22} - Z_{12}Z_{21}}{Z_{11}}\right] I_1 \tag{9}$$
$$Z_{TL}\big|_{\substack{Z_L=0 \\ S \ll}} = j\ Z_0 \tan(\beta h) \tag{10}$$
6. For the antenna mode with thin driven-shorting post, $Z_{11} = Z_{22}$ and $Z_{12} = Z_{21} \approx 0$, so Eq. (9) becomes:
$$V_2 = Z_{11}\ I_1 \approx Z_{22}\ I_1 \tag{11}$$

excited differently. To create the full radiation pattern, individual pixels and nearby pixel patches must be coupled along the radiating edge. To test how well the suggested design at $f = 5.32$ GHz performs with various gap distances between the elements, simulations are carried out with 5×5, 10×10, 20×20, 40×40, 80×80, and 100×100 pixels with the same amplitude and phase. A sample of the proposed pixel antenna array's 3D gain and total field radiation patterns (RPs) are shown in Fig. 8. This calculation is known as the array factor. The focus of array theory, which primarily focuses on combining array factors, is how a specific pattern is created. The central support structure for the self-adapting antenna will then be described and designed as the pixel antenna array. Radiating elements, also known as $Nx \times Ny$ proposed pixel patch elements, are distributed evenly along the x and y directions at uniform intervals of dx and dy. The proposed antenna array is divided into square pixels in Fig. 8.

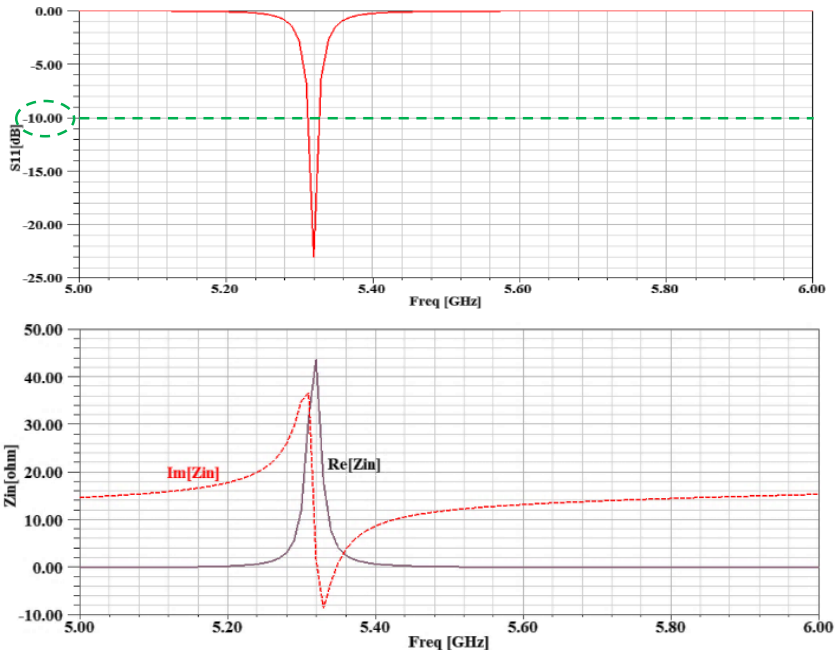

(a)

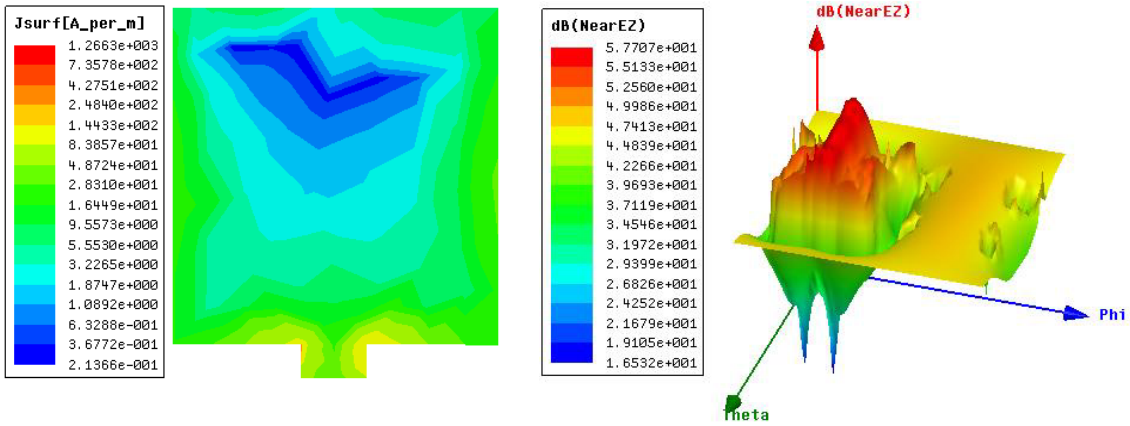

(b)

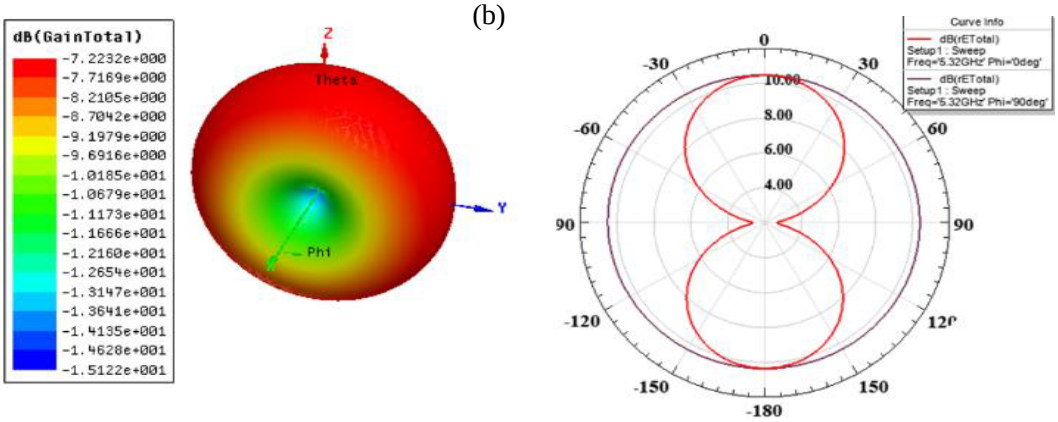

(c)

Figure 6. The proposed pixel patch element scattering parameters and radiation characteristics. (a) S_{11} [dB], and Z_{in} [ohms], (b) near-field, E_z, and current distribution, $J_{surf.}$, and (c) 3D gain and total field.

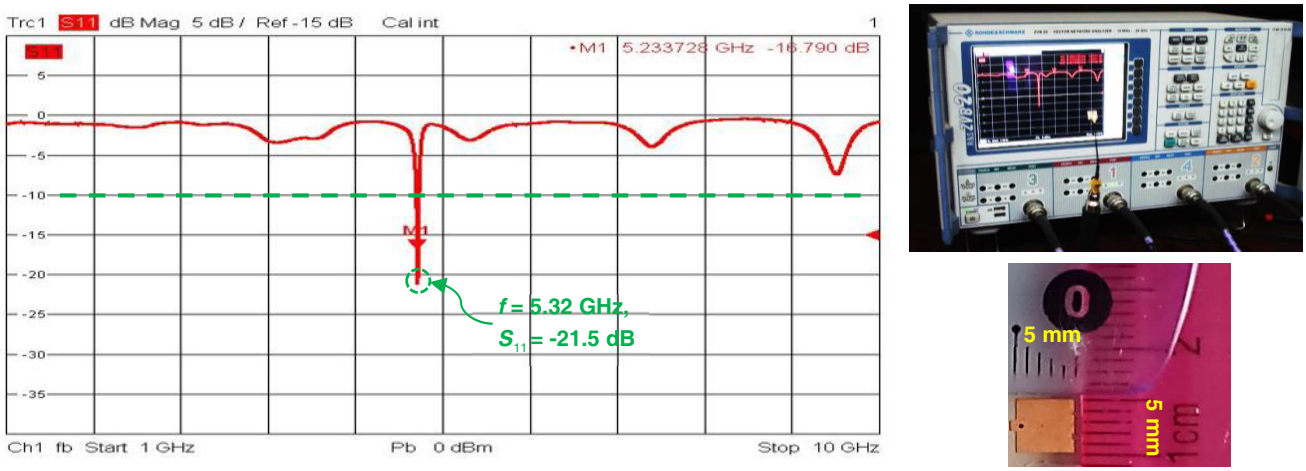

Figure 7. The fabricated sample of the proposed pixel patch antenna element configuration and measurement results.

Table 3. Comparison of sample literature methods with the proposed pixel patch antenna.

Ref. No.	Design Type	Freq. [GHz]	Dielectric Constant/ Thickness [mm]	Miniaturization Method	Patch Area [mm^2]	Design Area [mm^2]	Design Size Reduction %
[23]	BPF	UWB	2.2/0.787	Multi-Mode Resonators (MMRs) and Complementary Split Ring Resonators (CSRRs)	-	36 × 7.7	35
[25]	BLC	0.64&1.57	3.5/0.762	Loaded Coupled Transmission Lines (LCTL) and Complementary Split Ring Resonators (CSRRs)	-	12 × 6	75&52
[34]	DC	5	4.4/1.524	Defected Ground Structure (DGS)		36 × 40	31
[35]	DC	5	4.4/1.6	Fractal Defected Ground Structure (FDGS)		35.86 × 40	26
[36]	Ant.	1.93	4.4/1.6	Defected Ground Structure (DGS)	35.5 × 27.5	70 × 55	25
[37]	BLC	0.75	2.2/0.381	Resonators	-	35.3 × 24.4	84
[40]	Ant.	2.4 & 3.5 & 5.5	4.4/1.6	Metamaterials and Defected Ground Structure (DGS)	40 × 40	80 × 80	24
[57]	Ant.	3.5	4.4/1.6	Defected Ground Structure (DGS)	17 × 13.4	34 × 26.8	54
[58]	Ant.	2.4	4.4/1.6	Genetic Algorithm	27.3 × 22 19.5 × 16.3	46.5 × 21.2 38.7 × 35.7	24.4 45.8
This Paper	Ant.	5.32	10.2/0.635	Driven-Shorting Post (DS-Post)	5 × 5	6 × 6	90

BPF: Band Pass Filter, **BLC**: Branch Line Coupler, **DC**: Directional Coupler, **Ant.**: Antenna.

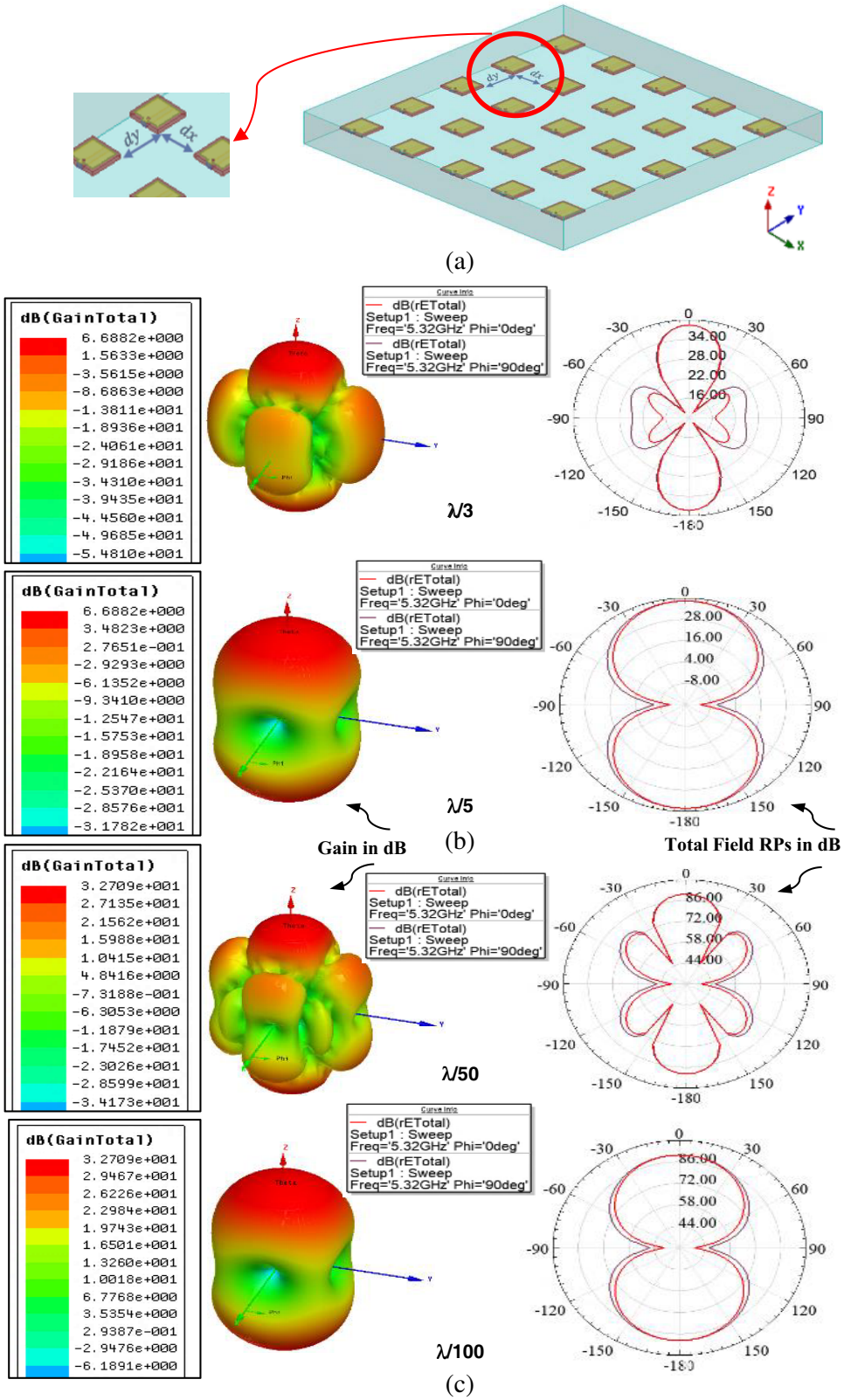

Figure 8. The proposed pixel antenna array and sample of the total field and gain for different spacing. (a) Design structure, (b) 5×5, (c) 100×100.

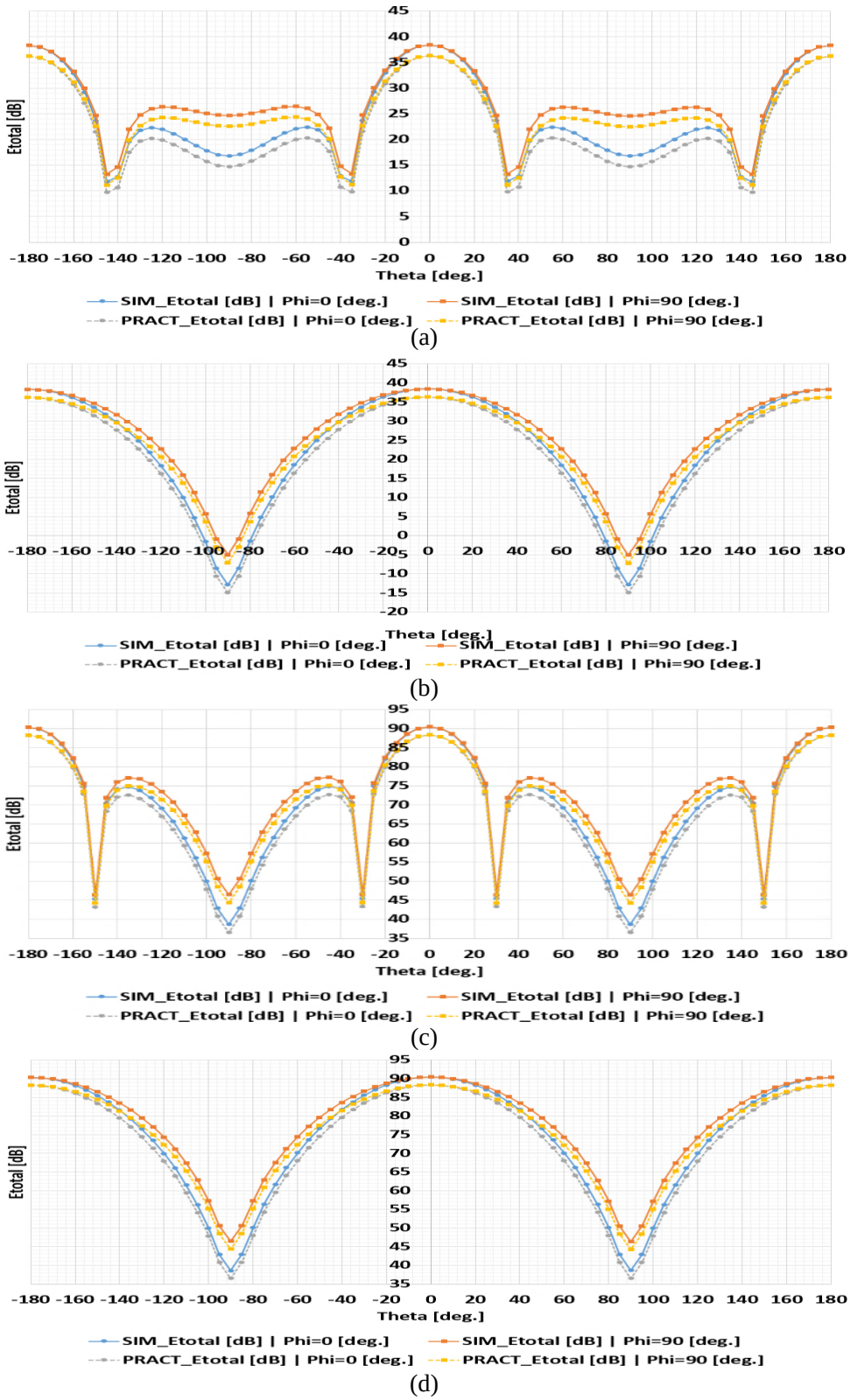

Figure 9. The proposed pixel antenna array simulation and practical comparison of the total field for different sample spacings. (a) 5×5 and $\lambda/3$, (b) 5×5 and $\lambda/5$, (c) 100×100 and $\lambda/50$, (d) 100×100 and $\lambda/100$.

Table 4. Summary of the proposed pixel antenna array design structures.

No. of pixel Elements ($Nx \times Ny$)	**Spacing between elements ($dx = dy$ mm)**	**Gain (dB)**	**Array Area (mm^2)**
5×5	$\lambda/4$ (14)	6.68	86×86
	$\lambda/3$ (18.6)		104.4×104.4
	$\lambda/5$ (11.2)		74.8×74.8
10×10	$\lambda/4$ (14)	12.7	186×186
	$\lambda/5$ (11.2)		160.8×160.8
	$\lambda/10$ (5.6)		110.4×110.4
20×20	$\lambda/4$ (14)	18.72	386×386
	$\lambda/10$ (5.6)		226.4×226.4
	$\lambda/20$ (2.8)		173.2×173.2
40×40	$\lambda/4$ (14)	24.75	786×786
	$\lambda/20$ (2.8)		349.2×349.2
	$\lambda/40$ (1.4)		294.6×294.6
80×80	$\lambda/4$ (14)	30.77	1586×1586
	$\lambda/40$ (1.4)		590.6×590.6
	$\lambda/80$ (0.7)		535.3×535.3
100×100	$\lambda/4$ (14)	32.7	1986×1986
	$\lambda/50$ (1.12)		710.8×710.8
	$\lambda/100$ (0.56)		655.4×655.4

Square pixel patches make up pixel antenna arrays. Every square pixel's distance from neighboring patches is measured in millimeters. The wavelength divided by half the total elements and the wavelength divided by the total elements are both equivalent to the x-y gap distance. The proposed pixel antenna array's frequency response is compared to the reference antennas once every pixel is wired up. A single pixel patch element's frequency response is identical to that of the entire pixel antenna array, and as more elements are added, the array's performance improves. Gain is measured using the logarithmic unit of decibels. The reference power is almost quadrupled by 6 dB, five times by 7 dB, etc. A two-dimensional radiation pattern represents gain on the plot. The radius of the plot in a decibel plot is normalized to the maximum value of the antenna. Pixels make up the proposed (collinear) antenna array. It was capable of four times the signal strength of a perfect dipole antenna, both for sending and receiving. Gain is affected by the separation between array elements. A narrower beamwidth results in higher gain, but in the proposed design, the beam is relatively wider than that in conventional designs. A larger beam may be required if numerous receiving units must remain connected.

The methodology behind the proposed antenna array is to use multiple omnidirectional structures that can be arranged vertically and linearly to maintain the same omnidirectional pattern in the azimuth plane but produce a more concentrated beam in the elevation plane with a higher gain. The proposed antenna array is frequently referred to as a collinear array. The antenna patterns are frequently depicted as plots in polar and rectangular coordinates, as demonstrated in Figs. 8 and 9. The lobes and nulls of the patterns in this picture show how the ground below an antenna can increase or decrease the intensity of the radiation, depending on the angle of vertical elevation. According to the results shown in Fig. 9 and Table 4, integrating the pixel element into the proposed antenna array affects the gain. A matching agreement has been reached between the simulation (SIM) and practical (PRACT) results, as demonstrated in Fig. 8. The gain will increase if the number of elements is increased, but it will not change if the distance between the elements is altered. Depending on how far apart each element is, the minor lobes that control the radiation pattern can be reduced or eliminated, which also improves

the appearance of the radiation pattern, which also improves the appearance of the radiation pattern. When the spacing and number of elements were considered, the minor lobes were completely removed, and the gain rose from 6.68 to 32.7 dB.

5. CONCLUSIONS

This paper introduces, investigates, and implements a miniaturized pixel antenna using a DS-post with a lower-order mode. The scattering parameters and the lower order mode resonant frequency at which perfect matching happens are affected by the length of the partially grounded microstrip TL and the position of the posts in the proposed pixel element. A network analyzer was used to measure the traditional patch antenna and proposed pixel patch element structures. Other methods from the literature were compared to the proposed pixel patch antenna to show how effective and useful the proposed DS-Post method in this paper is. Compared to traditional patches, the proposed pixel patch design area reduction is approximately 75%, and the full design area reduction is approximately 90%. The proposed pixel antenna array is smaller than the traditional microstrip array with high gain and a relatively wide beam, so it can be used in small space devices and miniaturized systems for communications, wireless networks, CubeSat, IoT, ADAS, and V2X applications.

REFERENCES

1. Liolis, K., A. Geurtz, R. Sperber,, et al., "Use cases and scenarios of 5G integrated satellite-terrestrial networks for enhanced mobile broadband: The SaT5G approach," *Int. J. Satell. Commun. Netw.*, Vol. 37, No. 2, 91–112, 2019.
2. Arifin, J., "Study of CUBESAT systems for IoT," *Proc. 12th Int. Renew. Eng. Conf. (IREC)*, 1–3, Apr. 2021.
3. Bassoli, R., F. Granelli, C. Sacchi, S. Bonafini, and F. H. Fitzek, "CubeSat based 5G cloud radion access networks: A novel paradigm for on-demand anytime/anywhere connectivity," *IEEE Veh. Technol. Mag.*, Vol. 15, No. 2, 39–47, 2020.
4. Centenaro, M., C. E. Costa, F. Granelli, C. Sacchi, and L. Vangelista, "A survey on technologies, standards and open challenges in satellite IoT," *IEEE Commun. Surveys Tuts.*, Vol. 23, No. 3, 1693–1720, 3rd Quart., 2021.
5. Padhi, P. K. and F. Charrua-Santos, "6G enabled industrial Internet of Everything: Towards a theoretical framework," *Appl. Syst. Innov.*, Vol. 4, No. 1, 11, Feb. 2021.
6. Ramahatla, K., M. Mosalaosi, A. Yahya, and B. Basutli, "Multiband reconfigurable antennas for 5G wireless and CubeSat applications: A review," *IEEE Access*, Vol. 10, 40910–40931, 2022.
7. Hu, P. F., K. W. Leung, Y. M. Pan, and S. Y. Zheng, "Electrically small, planar, horizontally polarized dual-band omnidirectional antenna and its application in a MIMO system," *IEEE Trans. Antennas Propag.*, Vol. 69, No. 9, 5345–5355, 2021, doi: 10.1109/TAP.2021.3061096.
8. Barman, B., D. Chatterjee, and A. N. Caruso, "Performance optimization of electrically small microstrip patch antennas on finite ground planes," *2020 IEEE Intern. Symp. on Ant. and Propag. and North American Radio Science Meeting*, 1–2, 2020.
9. Chen, X., M.-C. Tang, D. Yi, and R. W. Ziolkowski, "An interdigitated structure-based, electrically small dipole antenna with enhanced bandwidth," *2020 IEEE International Symposium on Antennas and Propagation and North American Radio Science Meeting*, 355–356, 2020.
10. Shameena, V. A., M. Manoj, M. Remsha, P. V. Anila, M. Sreejith Nair, and P. Mohanan, "Wideband electrically small monopole antenna," *2020 XXXIIIrd General Assembly and Scientific Symposium of the International Union of Radio Science*, 1–3, 2020.
11. Barman, B., K. C. Durbhakula, B. Bissen, D. Chatterjee, and A. N. Caruso, "Performance optimization of a microstrip patch antenna using characteristic mode and D/Q analysis," *2020 XXXIIIrd General Assembly and Scientific Symposium of the International Union of Radio Science*, 1–4, 2020.

12. Yu, Y.-H., Z.-Y. Zong, W. Wu, and D.-G. Fang, "Dielectric slab superstrate electrically small antennas with high gain and wide band," *IEEE Antennas Wireless Propag. Lett.*, Vol. 19, No. 9, 1476–1480, Sept. 2020.
13. Shubbar, M. and B. Rakos, "A self-adapting, pixelized planar antenna design for infrared frequencies," *Sensors*, Vol. 22, 3680, 2022, https://doi.org/10.3390/s22103680.
14. Garg, R., P. Bhartia, I. Bahl, and A. Ittipiboon, *Microstrip Antenna Design Handbook*, Artech House, Inc., Boston, London, 2001.
15. Ramesh, M. and K. B. Yip, "Design formula for inset fed microstrip patch antenna," *Journal of Micro. and Opt.*, Vol. 3, No. 3, 5–10, Dec. 2003.
16. Saturday, J. C., K. M. Udofi, and A. B. Obot, "Compact rectangular slot patch antenna for dual frequency operation using inset feed technique," *Intern. Journal of Information and Communication Sciences*, Vol. 1, No. 3, 47–53, Jan. 2017.
17. "ANSYS electronics desktop package," ANSYS v18, Ansoft Corporation.
18. Madany, Y. M., H. M. Elkamchouchi, and S. I. Abd-Elmonieum, "Frequency-tunable electrically small diversity patch antennas for cognitive radio applications," *2021 Inter. Telecommunications Conf. (ITC-Egypt)*, 1–6, 2021.
19. Khan, M. U., M. S. Sharawi, and R. Mittra, "Microstrip patch antenna miniaturization techniques: A review," *IET Microwaves, Antennas & Propagation*, Vol. 9, 913–922, 2015.
20. El Hachimi, Y., Y. Gmih, E. Makroum, and A. Farchi, "A miniaturized patch antenna designed and manufactured using slot's technique for RFID UHF mobile applications," *International Journal of Electrical and Computer Engineering (IJECE)*, Vol. 8, No. 6, 5134–5143, Dec. 2018.
21. Nagabhushana, H. M., C. R. Byrareddy, N. Thangadurai, and S. U. Sharief, "Slotted and miniaturized patch antenna for WLAN and WiMAX applications," *International Journal of Advanced Information Science and Technology (IJAIST)*, Vol. 6, No. 4, Apr. 2017.
22. Balanis, C. A., *Antenna Theory: Analysis and Design*, 3rd Edition, John Wiley & Sons, Inc., 2005.
23. Borazjani, O., M. Nosrati, and M. Daneshmand, "A novel triple notch-bands ultra wide-band band-pass filters using parallel multi-mode resonators and CSRRs," *International Journal of RF and Microwave Computer-Aided Engineering*, Vol. 24, No. 3, 375–381, 2014.
24. Pozar, D. M., *Microwave Engineering*, 4th Edition, John Wiley & Sons, 2012.
25. Hayati, M. and M. Nosrati, "Loaded coupled transmission line approach of left-handed (LH) structures and realization of a highly compact dual-band branch-line coupler," *Progress In Electromagnetics Research C*, Vol. 10, 75–86, 2009.
26. Rezaei, A. and L. Noori, "Microstrip hybrid coupler with a wide stop-band using symmetric structure for wireless applications," *Journal of Microwaves, Optoelectronics and Electromagnetic Applications*, Vol. 17, No. 1, Mar. 2018.
27. Sarkar, S., A. D. Majumdar, S. Mondal, S. Biswas, D. Sarkar, and P. P. Sarkar, "Miniaturization of rectangular microstrip patch antenna using optimized single-slotted ground plane," *Microwave Opt. Technol. Lett.*, Vol. 53, No. 1, 111–115, 2011.
28. Sarkar, M. and S. K. Chowdhury, "A new compact microstrip patch antenna," *Microwave Opt. Technol. Lett.*, Vol. 47, No. 4, 379–381, 2005.
29. Prabhakar, H. V., U. K. Kummuri, R. M. Yadahalli, and V. Munnappa, "Effect of various meandering slots in rectangular microstrip antenna ground plane for compact broadband operation," *Electron. Lett.*, Vol. 43, No. 16, 16–17, 2007.
30. Lin, S.-Y. and K.-C. Huang, "A compact microstrip antenna for GPS and SCS application," *IEEE Trans. Antennas Propag.*, Vol. 53, No. 3, 1227–1229, 2005.
31. Kuo, J.-S. and K.-L. Wong, "A compact microstrip antenna with meandering slots in the ground plane," *Microwave Opt. Technol. Lett.*, Vol. 29, No. 2, 95–97, 2001.
32. Er-Rebyiy, R., J. Zbitou, A. Tajmouati, M. Latrach, A. Errkik, and L. El Abdellaoui, "A new design of a miniature microstrip patch antenna using defected ground structure DGS," *2017 International Conference on Wireless Technologies, Embedded and Intelligent Systems (WITS)*, 1–4, 2017.

33. Pandhare, R. A., P. L. Zade, and M. P. Abegaonkar, "Miniaturized microstrip antenna array using defected ground structure with enhanced performance," *Engineering Science and Technology, An International Journal*, Vol. 19, No. 3, 1360–1367, 2016.
34. Bhakhar, P., V. Dwivedi, and P. Prajapati, "Directivity enhancement of miniaturized directional coupler using defected ground structure," *Proceedings of the International Conference on Communication and Signal Processing 2016 (ICCASP 2016)*, Advances in Intelligent Systems Research, Dec. 2016.
35. Bhakhar, P. and V. Dwivedi, "Symmetrical impedance microstrip coupled line coupler using fractal DGS for lower C-band applications," *International Journal of Microwave and Optical Technology*, Vol. 13, No. 2, 159–166, 2018.
36. Sanega, A. and P. Kumar, "A compact microstrip patch antenna for mobile communication applications," *Micro-Electronics and Telecommunication Engineering*, D. K. Sharma, V. E. Balas, L. H. Son, R. Sharma, K. Cengiz, Lecture Notes in Networks and Systems, Vol. 106, Springer, Singapore, 2020.
37. Roshani, S., S. I. Yahya, S. Roshani, and M. Rostami, "Design and fabrication of a compact branch-line coupler using resonators with wide harmonics suppression band," *Electronics, MDPI*, Vol. 11, 793, 2022.
38. Rani, R., P. Kaur, and N. Verma, "Metamaterials and their applications in patch antenna: A review," *International Journal of Hybrid Information Technology*, Vol. 8, No. 11, 199–212, 2015.
39. Nelaturi, S. and N. P. Venkata, "A compact microstrip patch antenna based on metamaterials for Wi-Fi and WiMAX applications," *Journal of Electromagnetic Engineering and Science*, Vol. 18, No. 3, 182–187, Jul. 2018.
40. Varamini, G., A. Keshtkar, and M. N. Moghadasi, "Compact and miniaturized microstrip antenna based on fractal and metamaterial loads with reconfigurable qualification," *AEU Inter. Jour. of Electronics and Communications*, Vol. 83, 213–221, 2018.
41. Li, R., G. Dejean, M. M. Tentzeris, and J. Laskar, "Development and analysis of a folded shorted-patch antenna with reduced size," *IEEE Trans. Antennas Propag.*, Vol. 52, No. 2, 555–562, 2004.
42. Chiu, C. Y., C. H. Chan, and K. M. Luk, "Study of a small wide-band patch antenna with double shorting walls," *IEEE Antennas Wireless Propag. Lett.*, Vol. 3, No. 1, 230–231, 2004.
43. Holub, A. and M. Polivka, "A novel microstrip patch antenna miniaturization technique: A meanderly folded shorted-patch antenna," *14th Conf. on Microwave Techniques*, 1–4, Apr. 2008.
44. Luk, K., R. Chair, and K. Lee, "Small rectangular patch antenna," *Electron. Lett.*, Vol. 34, No. 25, 2366, 1998.
45. Moon, S.-M., H.-K. Ryu, J.-M. Woo, and H. Ling, "Miniaturization of $\lambda/4$ microstrip antenna using perturbation effect and plate loading for low-VHF-band applications," *Electron. Lett.*, Vol. 47, No. 3, 162, 2011.
46. Porath, R., "Theory of miniaturized shorting-post microstrip antennas," *IEEE Trans. Antennas Propag.*, Vol. 48, No. 1, 41–47, 2000.
47. Mishra, A., P. Singh, N. P. Yadav, J. Ansari, and B. Vishvakarma, "Compact shorted microstrip patch antenna for dual-band operation," *Progress In Electromagnetics Research C*, Vol. 9, 171–182, 2009.
48. Wang, S., H. W. Lai, K. K. So, and K. B. Ng, "Wideband shorted patch antenna with a modified half U-slot," *IEEE Antennas Wireless Propag. Lett.*, Vol. 11, 689–692, 2012.
49. Waterhouse, R., S. Targonski, and D. Kokotoff, "Design and performance of small printed antennas," *IEEE Trans. Antennas Propag.*, Vol. 46, No. 11, 1629–1633, 1998.
50. Souza, E. A. M., P. S. Oliveira, A. G. D'Assunção, L. M. Mendonça, and C. Peixeiro, "Miniaturization of a microstrip patch antenna with a koch fractal contour using a social spider algorithm to optimize shorting post position and inset feeding," *Hindawi Publishing Corporation, International Journal of Antennas and Propagation*, Vol. 2019, Article ID 6284830, 10 pages, 2019.

51. Rathod, S. M., R. N. Awale, and K. P. Ray, "Shorted circular microstrip antennas for 50 Ω microstrip line feed with very low cross polarization," *Progress In Electromagnetics Research Letters*, Vol. 74, 91–98, 2018.
52. Salih, A. A. and M. S. Sharawi, "A dual-band highly miniaturized patch antenna," *IEEE Antennas Wireless Propag. Lett.*, Vol. 15, 1783–1786, 2016.
53. Menga, F. and S. Sharma, "Single feed dual-band (2.4 GHz/5 GHz) miniaturized patch antenna for wireless local area network (WLAN) communications," *Journal of Electromagnetic Waves and Applications*, 2016.
54. Boukarkar, A., X. Q. Lin, Y. Jiang, and Y. Q. Yu, "Miniaturized single-feed multiband patch antennas," *IEEE Trans. Antennas Propag.*, Vol. 65, No. 2, 850–854, Feb. 2017.
55. Ramzan, M. and K. Topalli, "A miniaturized patch antenna by using a CSRR loading plane," *Hindawi Publishing Corporation, International Journal of Antennas and Propagation*, Vol. 2015, Article ID 495629, 9 pages, 2015.
56. Painam, S. and C. Bhuma, "Miniaturizing a microstrip antenna using metamaterials and metasurfaces [Antenna applications corner]," *IEEE Antennas and Propagation Magazine*, Vol. 61, No. 1, 91–135, Feb. 2019.
57. Chakraborty, S., M. Gangapadhyaya, B. Sinha, and M. Chakraborty, "Miniaturization of rectangular microstrip antenna at WiMAX band with slot in patch and ground surface," *2018 2nd International Conference on Electronics, Materials Engineering & Nano-Technology (IEMENTech)*, 1–5, Kolkata, India, 2018.
58. Dhakshinamoorthi, M. K., S. Gokulakkrizhna, M. Denesh Kumar, et al., "Rectangular microstrip patch antenna miniaturization using improvised genetic algorithm," *2020 4th International Conference on Trends in Electronics and Informatics (ICOEI)*, 894–898, Tirunelveli, India, 2020.